# Carbon Nanotube-Templated Synthesis of Covalent Porphyrin Network for Oxygen Reduction Reaction

Ismail Hijazi, Tiphaine Bourgeteau, Renaud Cornut, Adina Morozan, Arianna Filoramo, Jocelyne Leroy, Vincent Derycke, Bruno Jousselme, and Stéphane Campidelli*

CEA Saclay, IRAMIS, NIMBE, Laboratoire d'Innovation en Chimie des Surfaces et Nanosciences (LICSEN), F-91191 Gif sur Yvette, France

Ⓢ Supporting Information

ABSTRACT: The development of innovative techniques for the functionalization of carbon nanotubes that preserve their exceptional quality, while robustly enriching their properties, is a central issue for their integration in applications. In this work, we describe the formation of a covalent network of porphyrins around MWNT surfaces. The approach is based on the adsorption of cobalt(II) *meso*-tetraethynylporphyrins on the nanotube sidewalls followed by the dimerization of the triple bonds via Hay-coupling; during the reaction, the nanotube acts as a template for the formation of the polymeric layer. The material shows an increased stability resulting from the cooperative effect of the multiple π-stacking interactions between the porphyrins and the nanotube and by the covalent links between the porphyrins. The nanotube hybrids were fully characterized and tested as the supported catalyst for the oxygen reduction reaction (ORR) in a series of electrochemical measurements under acidic conditions. Compared to similar systems in which monomeric porphyrins are simply physisorbed, MWNT−CoP hybrids showed a higher ORR activity associated with a number of exchanged electrons close to four, corresponding to the complete reduction of oxygen into water.
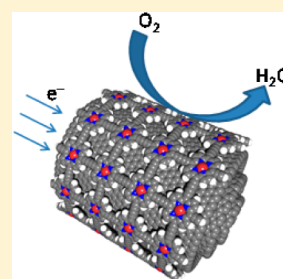
INTRODUCTION

The fabrication of functional hybrid materials that preserves and combines the properties of their building blocks is a central issue of nanosciences. Among the different classes of nanomaterials, carbon nanotubes are one of the most promising for solar energy conversion,[1−3] catalysis[4,5] and composite applications.[6,7] Within the context of sustainable development and renewable energy, we and others envisioned the use of functionalized or doped carbon nanotubes in electrocatalytic systems.[5,8−15] In such systems, the catalytic sites, which can be made of metallic nanoparticles, organometallic complexes, or any chemical functional group, need to be supported on conducting materials. Carbon nanotubes, thanks to their electrical conductivity and their high surface area (typically >200 m^2/g), appear as the ideal material for that purpose. In order to ensure an intimate mixing between the conducting support and the active sites, chemical methods based on covalent or noncovalent approaches are extremely promising. It is well established that the covalent grafting[16,17] of molecules onto the nanotube sidewalls gives rise to robust assemblies since the nanotubes and the addends are linked through covalent bonds; however, the transformation of carbon atoms hybridized sp^2 into sp^3 in the nanotube framework induces a sizable loss of their electronic properties. On the contrary, the noncovalent approach[18−20] permits better preservation of the electronic properties of the nanotubes but the weak interactions (π-stacking, hydrophobic, etc.) result in a lack of stability of the assemblies. Therefore, the development of techniques that offers a good control of the grafting while preserving the original properties of the building blocks is highly desirable.

In this work we developed an alternative method to combine carbon nanotubes with catalytic species for the oxygen reduction reaction (ORR). The reduction of oxygen into water is the reaction that takes place at the cathode of a fuel cell. The reaction is generally performed in the presence of platinum nanoparticle catalysts. The cost and scarcity of platinum encourage the development of new catalysts based on non-noble metals.[5,21] For example, in nature, the reduction of oxygen is performed by iron porphyrins in the active center of cytochrome coenzymes oxidase. Thus, bioinspired catalysts based on phthalocyanines and porphyrins derivatives mimicking the structure of the coenzyme have been extensively studied for oxygen reduction reaction (ORR).[22,23] In particular, iron phthalocyanines show high activity vs ORR with a four-electron reduction process;[23−25] unfortunately these macrocycles suffer from demetalation in the reaction media.[26,27] Very early, Jansinski demonstrated that cobalt phthalocyanines could efficiently reduce oxygen.[28] As a matter of fact, cobalt phthalocyanine and porphyrin catalysts are more stable than iron macrocycles but favor a two-electrons process[29,30] with production of hydrogen peroxide that degrades the carbon material support and decreases the fuel cell performances in the long run. During the past decade, several studies focused on the improvement of the reaction using cobalt macrocycles and it was found that cofacial cobalt *bis*-porphyrins (called the *Pacman* system) were able to reduce oxygen directly into water via a four-electron process.[31,32] However, because of the

complexity of their synthesis, the *Pacman bis*-porphyrin catalysts were only investigated in fundamental electrochemical experiments. Recently, Olaya et al. showed that the electrostatic face-to-face assembly of positively and negatively charged Co(II)−porphyrins performed the reduction of oxygen directly into water;[33] this work suggested that the design of well-defined structures is not mandatory to perform an efficient 4 e⁻ reduction. Then, in order to mimic easily and efficiently the cofacial *bis*-porphyrin system, we developed a new approach based on the cooperative effect of a multilayered cobalt porphyrin polymer. Herein, a covalent network of porphyrins was synthesized around the nanotube sidewalls: (i) to provide strong interactions between the carbon support and the macrocycles and (ii) to promote the formation of supra-molecular architectures, through the interactions between the macrocycles in the different layers. We believe that oxygen can be complexed and reduced similarly to what is observed in cofacial porphyrin systems.

Our method is based on the templated polymerization of a *meso*-tetraethynylporphyrin around multi-walled carbon nanotubes (MWNTs) via Hay-coupling.[34] This approach leads to carbon nanotube/porphyrin hybrids exhibiting high stability. Indeed, the resulting porphyrin polymer forms a homogeneous film on the nanotube surfaces, and the hybrids can be purified, manipulated, and dispersed in various solvents without loss of their functionality. The polymer around the nanotubes is made of several layers of porphyrins which can form cofacial complexes, thus increasing significantly the number of electrons (up to 3.93) during the reduction compared to physisorbed monomeric systems.

■ RESULTS AND DISCUSSION

The synthesis of MWNT-CoP **1** and cobalt porphyrin (CoP) derivative **2** are described in Scheme 1. *Note that the representation given in the Scheme is an idealized view of the reality; microscopic characterization (vide infra) shows that the porphyrins form an amorphous polymer coating around the nanotube sidewalls.* The trimethylsilane-protected Co(II) tetraethynylporphyrin **3** was synthesized from *meso*-tetra-(trimethylsilylethynyl)porphyrin **4** following literature procedures,[35,36] and then the alkyne functional groups were deprotected in the presence of tetrabutylammonium fluoride to give **2**. MWNTs were dispersed in *N*-methylpyrrolidone (NMP), then CoP **2** in NMP was added and gently sonicated, and then left to sit for 30 min. Copper(I) chloride and *N,N,N′,N′*-tetramethylethylenediamine (TMEDA) were added, and the reaction was stirred at room temperature for 24 h under an atmosphere of oxygen. After reaction, the nanotube derivatives were purified by filtration and extensive washing with NMP, tetrahydrofuran (THF), water, and ammonium hydroxide solution to remove the reagents and the copper catalyst. The polymer around the nanotubes exhibits a good stability; indeed after purification, the nanotube−porphyrin hybrid can be redispersed in common organic solvents such as NMP, *N,N*-dimethylformamide (DMF), and to a lower extent THF without loss of the grafting material.

The combination of carbon nanotubes with linear ethynyl-based porphyrin oligo/polymers has already been reported in the literature.[37−39] In the work described so far, the porphyrin derivatives were prepared separately and mixed with nanotubes afterward. Our approach is radically different, first because tetraethynyl porphyrins were used, and second because the polymerization is performed *in situ* on the nanotubes that serve

Scheme 1. Synthesis and Representation of MWNT−CoP.[a]
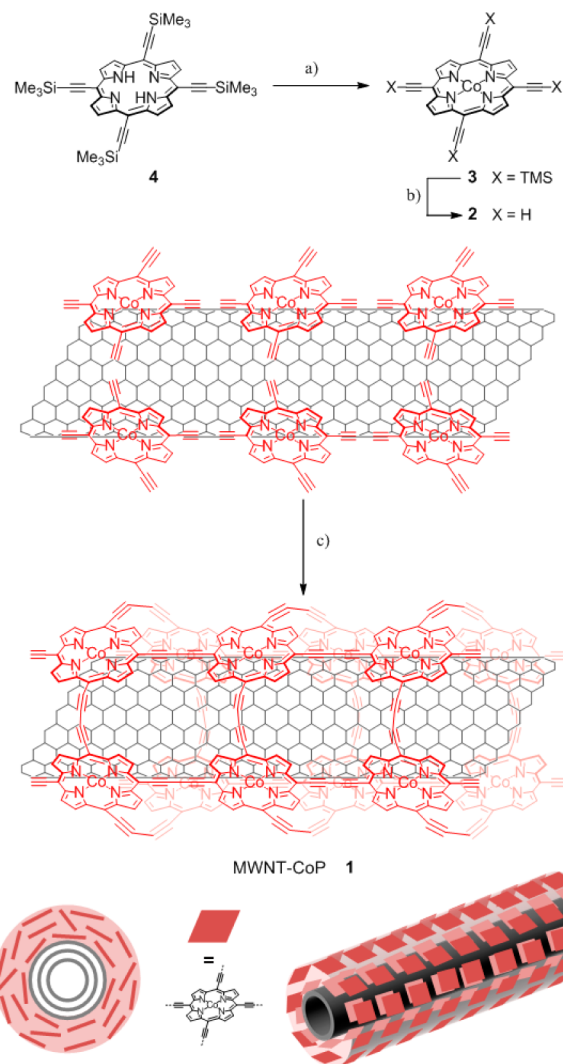
[a]Reagents and conditions: a) Co(OAc)₂, 4 H₂O, DMF, 120 °C, 1h, 86%; b) TBAF, THF, 0 °C, 95%; c) CuCl, TMEDA, NMP, rt. Bottom part: schematic representation of the nanotubes coated with the porphyrin polymer.

as templates for the reaction. The nanotubes used in this work were received from Nanocyl (MWNTs - NC3100), they exhibit an average diameter of ∼9.5 nm. These diameters are compatible with the formation of bent structures around the nanotubes by coupling between two triple bonds. Indeed, the butadiyne linker is extremely flexible, and rings of porphyrins containing down to six or eight monomers (diameters of ∼2.5 and 3.4 nm, respectively) were reported.[40,41]

The MWNT-CoP derivatives were characterized by a combination of absorption, Raman, X-ray photoelectron spectroscopy (XPS) and scanning and transmission electron microscopy (SEM, TEM). Figure 1a shows the absorption spectra of the porphyrin monomer **3** and MWNT-CoP **1** after polymerization. The spectrum of CoP exhibits three bands: the Soret at 465 and two Q-bands at 601 and 646 nm in NMP. The signal of the porphyrin in the nanotube hybrid is considerably broadened (band at 480 nm with a shoulder at ∼675 nm) and red-shifted, clearly indicating the formation of conjugated porphyrin oligomers/polymers.[42]
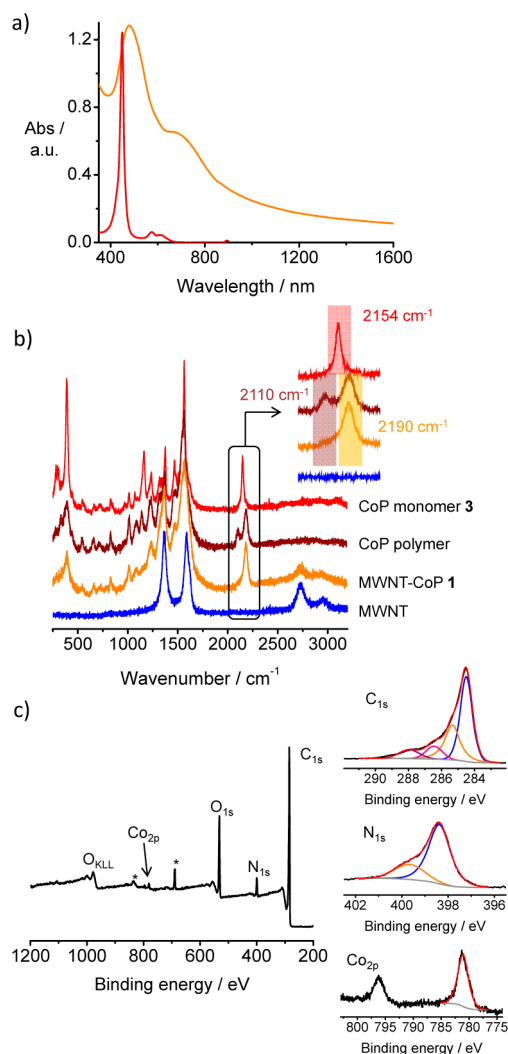
Figure 1. (a) absorption spectra of CoP **3** (red) and MWNT-CoP **1** (orange) in NMP; the Soret and Q bands of the porphryin are broadened and red-shifted after polymerization. (b) Raman spectra of MWNT (blue), MWNT-CoP **1** (orange), Co-porphyrin polymer without nanotubes (brown), and CoP **3** (red). The inset shows the evolution of the stretching of the C≡C bonds. (c) XPS spectrum of MWNT-CoP **1** and deconvoluted XPS core level spectra of carbon C_{1s}, N_{1s}, and Co_{2p} of **1**. The signals noted "*" are due to fluorine atoms (F_{1s} and F_{KLL}) from the polytetrafluoroethylene (PTFE) supporting membrane.

The Raman spectra of MWNTs, MWNT-CoP **1**, CoP polymer (reference polymer synthesized in the absence of nanotubes), and porphyrin **3** are shown in Figure 1b. The comparison between the spectra confirms the formation of a covalent network of porphyrins around the nanotube sidewalls. In the 250 and 1750 cm^{-1} region, the spectrum of MWNT-CoP **1** is dominated by the signals of the porphyrin, while the presence of MWNT is confirmed by the 2D and D+D′ bands at ~2730 and 2950 cm^{-1}, respectively. The spectra of the porphyrin-containing derivatives also exhibit interesting features between 2100 and 2200 cm^{-1}; this region is known to be the one where the triple bond stretching mode is observed. The band at 2154 cm^{-1} (red spectrum) was attributed to the vibration of the protected acetylene moieties in CoP **3**. After deprotection and polymerization this band disappears and gives two bands at ~2110 and 2190 cm^{-1} that

was attributed to the ethynyl and 1,3-butadiynyl moieties, respectively. Note that in **1** the band at 2110 cm^{-1} is almost nonexistent, it only forms a shoulder on the left of the 2190 cm^{-1} stretching band. This observation suggests that the alkyne groups of CoP **3** strongly participate in the formation of the porphyrin film around the surface of MWNT and that there are almost no ethynyl pendant groups remaining.

Quantitative analyses of the nanotube−porphyrin hybrids were performed by means of XPS. The spectrum of MWNT−CoP **1** (Figure 1c) shows the presence of carbon, oxygen, nitrogen, and cobalt in the hybrid. The deconvolution of the C_{1s} energy level signals, for **1**, was performed with four Gaussian−Lorentzian curves which were attributed to the various carbon atoms (Csp and Csp^2, Csp^3, C=O, and CO_2H) present in the nanotubes and the porphyrins. The deconvolution of the N_{1s} energy level signals, for **1**, was performed with two peaks at 398.3 and 399.7 eV, respectively. The first peak was attributed to the nitrogen of the porphyrin, while the second peak was attributed to the residual NMP which filled the nanotubes during the reaction.[43,44] The complete listing of the binding energies is reported in Table S1 of Supporting Information [SI]. We estimated the average number of porphyrins on the nanotubes (with the ratio of the peak areas $C_{1s}/Co_{2p3/2}$ - see Table S1 of SI) to 1 cobalt atom for 130 carbon atoms, corresponding to 1 porphyrin for 102 carbon atoms of the nanotube (CoP contains 28 C atoms). This result shows that a large number of porphyrins were immobilized on the nanotubes, and we can assume that the porphyrins form a multilayer around the outer wall. For example using simple geometric considerations (see SI for the detail of the estimation), a 1 nm section of a MWNT of 9.5 nm diameter and containing 8 walls which corresponds roughly to 280 carbon atoms.

In order to compare the properties of MWNT−CoP **1** to those of reference materials, we prepared a MWNT/CoP hybrid in which monomeric *meso*-tetra(trimethylsilylethynyl)-porphyrinato cobalt(II) derivative was simply mixed with nanotubes as described previously (Figure S2 of SI).[25] The absorption, Raman, and the XPS spectra of the hybrid are given in Figure S3 of SI. The absorption spectrum of the hybrid is dominated by the signal of the porphyrin, and the contribution of the nanotubes is identified by the weak and continuous absorption in the near-infrared region (800−1600 nm). Raman spectrum of MWNT/CoP is very similar to that of MWNT−CoP **1**; it shows the presence of porphyrins (in the low wavenumber region) and of nanotubes with the 2D and D+D′ bands between 2700 and 3000 cm^{-1}. The main difference comes from the bands associated with the stretching mode of the triple bond; the latter appears at 2151 cm^{-1} (C≡C−$SiMe_3$). Finally, the XPS spectrum shows the presence of silicon (from TMS), carbon, nitrogen, oxygen, and cobalt. By comparing the signal of carbon and cobalt (vide supra), we estimated that the physisorbed MWNT/CoP hybrid contained 1 cobalt atom for 135 carbon atoms (which corresponds to 1 porphyrin **3** for 95 carbon atoms of the nanotubes).

Microscopic analyses of MWNT-CoP **1** were performed by SEM and TEM (Figure 2); the images confirmed the high amount of porphyrin on the nanotubes. The electron micrographs show that the general aspect of the pristine and functionalized nanotubes is similar in terms of diameter and length. However, compared to pristine MWNTs, MWNT−CoP **1** are covered by a relatively thin layer of polymer. This polymeric material is made of multilayers of cobalt porphyrins;
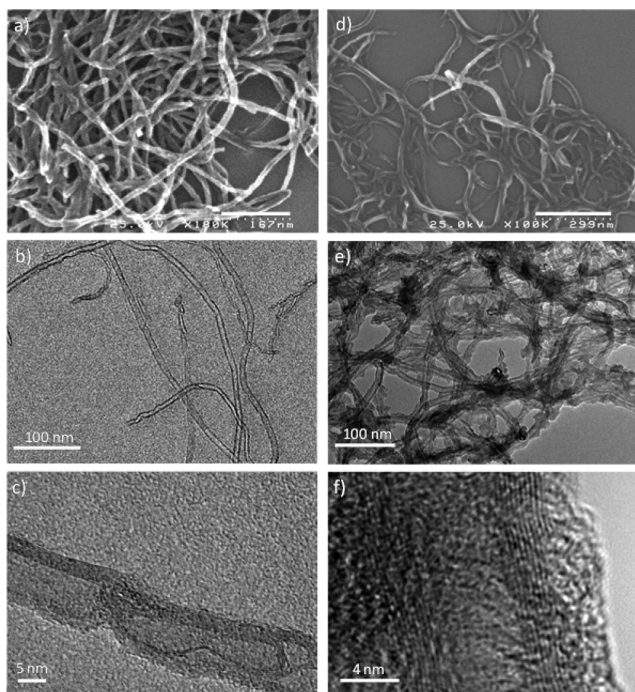
Figure 2. SEM (a) and TEM (b,c) micrographs of pristine MWNTs; SEM (d) and TEM (e,f) micrographs of MWNT−CoP **1**. The images show clearly the presence of a polymeric layer around the functionalized MWNTs.

they are exclusively located around the nanotube sidewalls and form an amorphous coating on the nanotube surfaces. In comparison, SEM and TEM images of the physisorbed MWNT/CoP hybrid are presented in Figure S4 of SI. SEM images of MWNT/CoP did not show the presence of an organic layer around the nanotubes; the porphyrin formed a kind of puddle on the silicon surface around the nanotubes. TEM images permitted distinguishing the presence of a layer of porphyrin around the nanotubes. This layer is thin and discontinuous and is due to the stacking of Co(II)tetra-(trimethylsilylethynyl)-porphyrin monomers on the nanotube sidewalls.

The porphyrin monomer interacts with the nanotube sidewalls by π-stacking. These interactions are relatively strong in the case of porphyrins without phenyl rings in the *meso* position; this can explain the very thin layer around the nanotubes observed by TEM (see SI). The porphyrins not interacting directly with the nanotubes stack weakly with each other and at least not sufficiently to give rise to a stable shell around the nanotubes. It is completely different for MWNT−CoP **1**: in **1**, the porphyrins are linked together via butadiyne linkers. It is likely that the first layer interacts with the nanotube by π-stacking interactions and that cross-linking between porphyrins in the different layers gives rise to formation of the porphyrin shell around the nanotubes.

The catalytic activity of the MWNT−CoP **1** toward ORR was tested in a series of rotating disk electrode (RDE) and rotating ring disk electrode (RRDE) measurements under acidic conditions. The results were compared to the ones obtained for bare MWNTs and MWNT/CoP hybrids. As demonstrated by XPS analyses, the amount of cobalt centers is almost equivalent in MWNT−CoP **1** and in MWNT/CoP hybrids allowing comparison of the catalytic properties of the two nanotube derivatives. The different samples were

formulated in an ink containing Nafion, ethanol, and water and were drop-casted at different loadings on glassy carbon disks. In contrast to the MWNT sample (Figure 3a, blue curve)
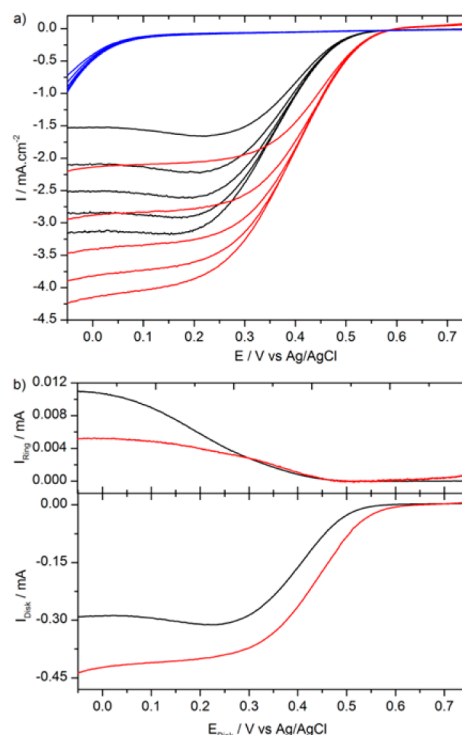

Figure 3. (a) Polarization curves at different rotation rates (400, 800, 1200, 1600, and 2000 rpm) recorded for ORR in O_2-saturated 0.5 M H_2SO_4 solution (scan rate =5 mV·s^{-1}, 25 °C) on GC with predeposited MWNT−CoP **1** (red), physisorbed MWNT/CoP (black), and MWNTs (blue) lines. The loading is 155 μg·cm^{-2}. (b) RRDE measurements for MWNT−CoP **1** (red) and physisorbed MWNT/CoP (black) (155 μg.cm^{-2}) in O_2-saturated 0.5 M H_2SO_4 (5 mV·s^{-1}, 400 rpm). The ring electrode was polarized at 1.2 V vs Ag/AgCl.

that does not show efficient catalytic oxygen reduction properties, the polarization curves of MWNT−CoP **1** in O_2-saturated 0.5 M H_2SO_4 solution show a reduction current starting at 0.55 V vs Ag/AgCl (Figure 3a, red curve) for different rotating rates that confirms the ORR activity of the hybrid. Similarly, the physisorbed MWNT/CoP reference sample (Figure 3a, black curve) presents catalytic activity toward ORR as previously reported,[25] but the onset potential is slightly lower (negatively shifted by 50 mV), and the current density at low potential is 20% lower than those of the MWNT−CoP **1** for the same catalyst loading (155 μg·cm^{-2} corresponding to 17 nmol of porphyrins). From these data, the mass transfer-corrected Tafel plots (Figure S5 of SI) show that the CoP assembly obtained with the templated polymerization process has an activity about 3.6 times higher than with the simple mixture of porphyrins and nanotubes. This difference was further assessed by RRDE analysis (Figure 3b) in order to determine the average reaction electron number (*n*) for MWNT−CoP **1** and physisorbed MWNT/CoP. The current detected at the ring for physisorbed MWNT/CoP is higher than the one for MWNT−CoP **1**, indicating a higher hydrogen peroxide production for the MWNT/CoP. The *n* values estimated from the RRDE measurements at −0.05 V vs Ag/AgCl with a catalyst loading of 155 μg·cm^{-2} are 3.35 and 3.82

for physisorbed MWNT/CoP and MWNT−CoP **1**, respectively.

In order to test the stability of the electrocatalytic activity, a chronoamperometry at 0.2 V vs Ag/AgCl in O_2-saturated H_2SO_4 solution was carried out for 24 h. As shown in Figure S6 of SI, the stability of the MWNT−CoP **1** is higher than that of the MWNT/CoP, with current decreasing respectively by 5% and 20% after 24 h. This result could be explained by the fact that MWNT−CoP **1** has a higher number of exchanged electrons (close to 4), so that less H_2O_2, that degrades the carbon material support, is produced.

Finally, the impact of the electrocatalyst loading on the *n* value was investigated by RRDE experiments.[45] At any catalyst loading, the number of electrons (Table 1) is always higher

Table 1. Average Electron Number *n* Extracted from RRDE Measurements for Different Catalyst Loadings of MWNT/CoP and MWNT−CoP 1

loading ($\mu g \cdot cm^{-2}$)	physisorbed MWNT/CoP	MWNT−CoP **1**
52	3.24	3.75
155	3.35	3.82
387	3.60	3.93

than 2, and higher for MWNT−CoP **1** than for physisorbed MWNT/CoP. Thus, both catalysts operate under combined $4e^-$ and $2e^-$ ORR processes, with a more predominant $4e^-$ pathway for MWNT−CoP **1**. The better results obtained in the case of MWNT−CoP **1** can be attributed to the presence of multilayers of porphyrin around the nanotubes which provides a configuration similar to the *Pacman bis*-porphyrin systems described by Nocera.[31]

■ CONCLUSION

We described the formation of a covalent network of cobalt−porphyrins on MWNT surfaces. This approach based on Hay coupling provides a robust method for noncovalent carbon nanotube functionalization. After reaction, the nanotubes are embedded in the porphyrin polymer and the multiple π−π interactions lead to stable assemblies that can be purified by filtration and redispersed without loss of the grafted materials. XPS and TEM analyses show that the nanotubes are covered by a multilayer of CoP; the porphyrins form an amorphous but robust film around the nanotubes.

The MWNT−CoP hybrid was tested for ORR in a series of electrochemical measurements under acidic conditions. The RRDE measurements showed improved catalytic performances of the material, with an average value of transferred electrons that was close to 4. We are now extending the method to other metalated porphyrins and phthalocyanines, and we are working on the control of the number of layers around the nanotubes to evaluate their influence on the reduction process.

■ EXPERIMENTAL SECTION

Techniques. UV−vis−NIR spectra were recorded in 1 cm quartz cuvettes on a Perkin Elmer Lambda 900 UV−vis−NIR spectrophotometer. FT-IR spectra were recorded on a Bruker Alpha FT-IR spectrometer. ^1H NMR spectra were recorded with a Bruker AC-300 (300 MHz) instrument with solvent used as internal reference. MALDI-TOF MS spectra were obtained from a Perseptive Biosystems Voyager DE-STR instrument. Raman spectra were collected by a T64000 Jobin-Yvon spectrometer (in triple or single configuration) through an optical microscope (Olympus BX41, objective 100×), choosing the excitation source among the lines of an Ar−Kr laser; the

spot size was about 1 μm. For X-ray photoelectron spectroscopy (XPS) a Kratos Analytical Axis Ultra DLD, using an Al Kα source monochromatized at 1486.6 eV was used. We used a hemispheric analyzer working at pass energy of 50 eV for the global spectrum, and 20 eV when focusing on the sole core levels. The samples were supported on PTFE membrane or on gold-coated glass. For SEM, the samples were prepared by drop casting from NMP or THF solutions on silicon substrates, and the images were performed on a SEM Hitachi S4500 operating at 25 or 15 kV. For TEM, the samples were prepared by drop casting from EtOH solutions on carbon-coated copper grids (Agar Scientific) and then imaged on a FEI TECMAI G2 Spirit Twin or on a JEOL 2010F electron microscope operating at 120 or 80 kV.

Electrochemical Experiments. ORR Experiments. Sample Preparation. MWNT-CoP **1** in solution in NMP was precipitated by addition of ethanol and then centrifuged; the supernatant was discarded, and the operation was repeated twice. The catalyst inks were prepared by sonicating 10 mg of the hybrid catalyst powders in 600 μL of a mixture of ethanol and water (3 for 1 in volume) and 60 μL of a commercial Nafion solution (5 wt % in alcohol).

Electrode Preparation. Before each measurement, the glassy carbon (GC) disk (5 mm, 0.196 cm^2) used as rotating electrode was polished with aqueous dispersions of synthetic diamonds (1 μm), then rinsed and sonicated with water. Each active layer was deposited from the catalyst inks by drop-casting onto the GC disk, then dried in air. The loading was modified by casting different volumes of ink and diluting inks in ethanol when necessary.

Electrochemical Measurements. The instrument used was a VSP bipotentiostat (Bio-Logic SAS). The electrochemical tests were carried out in 0.5 M H_2SO_4 solution in a three electrode glass cell, thermostated at 25 °C. A "CE to Ground" connection with a saturated KCl Ag/AgCl electrode as reference and a graphite plate as counter electrode was used. As a working electrode, a Pine rotating ring disk electrode (RRDE) with catalyst-loaded GC disk (0.196 cm^2) and Pt ring (0.110 cm^2) was controlled by a speed control unit from Princeton Applied Research model 636 electrode rotator. The voltammograms were recorded at 5 mV·s^{-1} in stationary conditions (with various rotating rates: 400, 800, 1200, 1600, and 2000 rpm) in O_2-saturated solutions. An average current was calculated from the forward and backward scans. All potentials reported in this paper refer to that of the Ag/AgCl electrode. H_2O_2 production was monitored in the RRDE configuration at 400 rpm with a cyclic voltammetry at the GC disk (5 mV·s^{-1}) and the Pt ring electrode held at 1.2 V vs Ag/AgCl.

The collection coefficient of the RRDE was measured using the one-electron $Fe(CN)_6^{3-}/Fe(CN)_6^{4-}$ redox couple, according to the manufacturer's instructions and keeping the current in mA. It was evaluated at 0.25 when the GC disk was loaded with MWCNT−CoP **1** and 0.22 with MWCNT/CoP physisorbed.

Materials. Chemicals were purchased from Aldrich and were used as received. Solvents were purchased form Aldrich or VWR and were used as received. For synthesis, CH_2Cl_2 (CaH_2, N_2), THF (K/benzophenone, N_2) were distilled before use. MWNT commercial grade NC3100 (>95%) were purchased from Nanocyl and purified by oxidative treatment at 100 °C for 4 h in 35% HNO_3. *meso*-tetra(trimethylsilylethynyl)porphyrin **4** was synthesized according to the literature procedure.[35]

Synthesis. *MWNTs.* MWNTs (40 mg) were sonicated in nitric acid (35 vol %) (150 mL) with a sonic bath (160 W max) (100% for 5 min and then 40% for 15 min) and then heated at 100 °C for 5 h. The suspension was then cooled and vacuum filtered through a 0.2 μm PTFE membrane and washed with water. The nanotubes were redispersed in NaOH 2 M (100 mL) using the sonic bath (100% for 10 min) and then filtered through a PTFE membrane and washed with deionized water, and then HCl 1 M followed by deionized water until the filtrate was neutral.

Porphyrin 3. A solution of $Co(OAc)_2$, 4 H_2O (100 mg, 0.400 mmol) was added to a solution of *meso*-tetra(trimethylsilylethynyl)-porphyrin **4** (100 mg, 0.144 mmol) in DMF (10 mL) in a 100 mL Schlenk flask equipped with a magnetic stir bar. The reaction mixture

was stirred for 1 h at 100 °C. After extraction, the combined organic fractions were dried over anhydrous $MgSO_4$ and then filtered. Then volatiles were removed from the reaction mixture under reduced pressure using a rotary evaporator. The crude product was purified by column chromatography (THF) to give **3** as a green solid (93 mg, 86%). Because **3** is paramagnetic, NMR was not performed. FT-IR (KBr) v (cm^{-1}) 3375, 2957, 2918, 2849, 1733, 1467, 1447, 1389, 1386, 1312, 1289, 1249, 1243, 1197, 1180, 1121, 1103, 1070, 1025, 988, 852, 796, 714. UV–vis (NMP) λ_{max} (nm) 449, 574, 610. MALDI-TOF MS m/z = 751.20 (M$^{+\bullet}$), Calcd for $C_{40}H_{44}CoN_4Si_4$: 751.18.

Porphyrin 2. Porphyrin **3** (40 mg, 0.053 mmol) was solubilized in THF (10 mL), and then a solution of tetrabutylammonium fluoride (TBAF) (250 μL of a 1 M solution inTHF) was added. After stirring for 1 h at room temperature and under nitrogen, 40 mL of water was added. The solution was concentrated under reduced pressure, filtered, and washed with water. After drying, the expected compound was obtained in 95% yield (24 mg). Because **2** is paramagnetic, NMR was not performed. FT-IR (KBr) v (cm^{-1}) 3310, 2924, 2855, 2113, 1722, 1611, 1563, 1460, 1362, 1349, 1255, 1236, 1226, 1163, 1121, 1068, 1010, 939, 885, 793, 707, 656, 588. UV–vis (NMP) λ_{max} (nm) 460, 588, 638. MALDI-TOF MS m/z = 463,04 (M$^+$), Calcd for $C_{28}H_{12}CoN_4$: 463.05.

MWNT–CoP 1. Porphyrin **2** (15 mg, 0.032 mmol) was added to a suspension of MWNTs (10 mg) in NMP (150 mL). To adsorb the porphyrin on the nanotube surface, the solution was gently sonicated and then left to sit for 30 min. Then a freshly prepared suspension of TMEDA (100 μL) and copper(I) chloride (25 mg, 0.25 mmol) in NMP (2 mL) was added before the air was bubbled into the solution. The reaction mixture was stirred overnight at room temperature under air. The suspension was filtered on a PTFE membrane (0.2 μm), and the solid was washed with NMP, deionized water, a solution of NH_3 (5%), and then water and NMP. In order to remove the eventual products absorbed on the nanotubes, the buckypaper was redispersed in NMP, then refiltered and washed with NMP, THF, and CH_2Cl_2. These operations were repeated until the filtrate contained no porphyrin (checked by UV–vis absorption).

■ ASSOCIATED CONTENT

Ⓢ Supporting Information

Description and characterization of physisorbed MWNT/CoP; details on the binding energies and the estimation of the number of carbon atoms per nm of nanotube; Tafel plots and chronoamperometry. This material is available free of charge via the Internet at http://pubs.acs.org.

■ AUTHOR INFORMATION

Corresponding Author
stephane.campidelli@cea.fr

Notes
The authors declare no competing financial interest.

■ ACKNOWLEDGMENTS

■ REFERENCES

(1) Ago, H.; Petritsch, K.; Shaffer, M. S. P.; Windle, A. H.; Friend, R. H. *Adv. Mater.* **1999**, *11*, 1281–1285.

(2) Umeyama, T.; Imahori, H. *Energy Environ. Sci.* **2008**, *1*, 120–133.

(3) Sgobba, V.; Guldi, D. M. *Chem. Soc. Rev.* **2009**, *38*, 165–184.

(4) Pumera, M. *Chem.—Eur. J.* **2009**, *15*, 4970–4978.

(5) Morozan, A.; Jousselme, B.; Palacin, S. *Energy Environ. Sci.* **2011**, *4*, 1238–1254.

(6) Spitalsky, Z.; Tasis, D.; Papagelis, K.; Galiotis, C. *Prog. Polym. Sci.* **2010**, *35*, 357–401.

(7) Sahoo, N. G.; Rana, S.; Cho, J. W.; Li, L.; Chan, S. H. *Prog. Polym. Sci.* **2010**, *35*, 837–867.

(8) Zhang, W.; Sherrell, P.; Minett, A. I.; Razal, J. M.; Chen, J. *Energy Environ. Sci.* **2010**, *3*, 1286–1293.

(9) Wu, B.; Kuang, Y.; Zhang, X.; Chen, J. *Nano Today* **2011**, *6*, 75–90.

(10) Liang, Y.; Li, Y.; Wang, H.; Dai, H. *J. Am. Chem. Soc.* **2013**, *135*, 2013–2036.

(11) Le Goff, A.; Artero, V.; Jousselme, B.; Tran, P. D.; Guillet, N.; Métayé, R.; Fihri, A.; Palacin, S.; Fontecave, M. *Science* **2009**, *326*, 1384–1387.

(12) Tran, P. D.; Le Goff, A.; Heidkamp, J.; Jousselme, B.; Guillet, N.; Palacin, S.; Dau, H.; Fontecave, M.; Artero, V. *Angew. Chem., Int. Ed.* **2011**, *50*, 1371–1374.

(13) Toma, F. M.; Sartorel, A.; Iurlo, M.; Carraro, M.; Parisse, P.; Maccato, C.; Rapino, S.; Rodriguez Gonzalez, B.; Amenitsch, H.; Da Ros, T.; Casalis, L.; Goldoni, A.; Marcaccio, M.; Scorrano, G.; Scoles, G.; Paolucci, F.; Prato, M.; Bonchio, M. *Nat. Chem.* **2010**, *2*, 826–831.

(14) Elouarzaki, K.; Le Goff, A.; Holzinger, M.; Thery, J.; Cosnier, S. *J. Am. Chem. Soc.* **2012**, *134*, 14078–14085.

(15) Zhao, H.; Zhang, Y.; Zhao, B.; Chang, Y.; Li, Z. *Environ. Sci. Technol.* **2012**, *46*, 5198–5204.

(16) Tasis, D.; Tagmatarchis, N.; Bianco, A.; Prato, M. *Chem. Rev.* **2006**, *106*, 1105–1136.

(17) Singh, P.; Campidelli, S.; Giordani, S.; Bonifazi, D.; Bianco, A.; Prato, M. *Chem. Soc. Rev.* **2009**, *38*, 2214–2230.

(18) Nakashima, N.; Tomonari, Y.; Murakami, H. *Chem. Lett.* **2002**, 638–639.

(19) Zhao, Y.-L.; Stoddart, J. F. *Acc. Chem. Res.* **2009**, *42*, 1161–1171.

(20) Britz, D. A.; Khlobystov, A. N. *Chem. Soc. Rev.* **2006**, *35*, 637–659.

(21) Jaouen, F.; Proietti, E.; Lefèvre, M.; Chenitz, R.; Dodelet, J.-P.; Wu, G.; Chung, H. T.; Johnston, C. M.; Zelenay, P. *Energy Environ. Sci.* **2011**, *4*, 114–130.

(22) Bezerra, C. W. B.; Zhang, L.; Lee, K.; Liu, H.; Marques, A. L. B.; Marques, E. P.; Wang, H.; Zhang, J. *Electrochem. Acta* **2013**, *53*, 4937–4951.

(23) Zagal, J. H.; Griveau, S.; Silva, J. F.; Nyokong, T.; Bedioui, F. *Coord. Chem. Rev.* **2010**, *254*, 2755–2791.

(24) Li, W.; Yu, A.; Higging, D. C.; Llanos, B. G.; Chen, Z. *J. Am. Chem. Soc.* **2010**, *132*, 17058.

(25) Morozan, A.; Campidelli, S.; Filoramo, A.; Jousselme, B.; Palacin, S. *Carbon* **2011**, *49*, 4839–4847.

(26) Meier, H.; Tschirwitz, U.; Zimmerhackl, E.; Albrecht, W.; Zeitler, G. *J. Phys. Chem.* **1977**, *81*, 712.

(27) Baraton, S.; Coutanceau, C.; Roux, C.; Hahn, F.; Léger, J.-M. *J. Electroanal. Chem.* **2005**, *577*, 223–234.

(28) Jasinski, R. *Nature* **1964**, *201*, 1212–1213.

(29) Zagal, J.; Paez, M.; Tanaka, A. A.; Dos Santos, J. R.; Likous, C. A. *J. Electroanal. Chem.* **1992**, *339*, 13–30.

(30) Steiger, B.; Anson, F. C. *Inorg. Chem.* **1995**, *34*, 3355–3357.

(31) Rosenthal, J.; Nocera, D. G. *Acc. Chem. Res.* **2007**, *40*, 543–553 and references therein.

(32) Peljo, P.; Murtomäki, L.; Kallio, T.; Xu, H.-J.; Meyer, M.; Gros, C. P.; Barbe, J.-M.; Girault, H. H.; Laasonen, K.; Kontturi, K. *J. Am. Chem. Soc.* **2012**, *134*, 5974–5984.

(33) Olaya, A. J.; Scaming, D.; Brevet, P.-F.; Nagatani, H.; Zimmermann, T.; Vanicek, J.; Xu, H.-J.; Gros, C. P.; Barbe, J.-M.; Girault, H. H. *J. Am. Chem. Soc.* **2012**, *134*, 498–506.

(34) Hay, A. S. *J. Org. Chem.* **1962**, *27*, 3320–3321.

(35) Anderson, H. L. *Tetrahedron Lett.* **1992**, *33*, 1101–1104.

(36) Armand, F.; Albouy, P.-A.; Da Cruz, F.; Normand, M.; Huc, V.; Goron, E. *Langmuir* **2001**, *17*, 3431–3437.

(37) Cheng, F.; Adronov, A. *Chem.—Eur. J.* **2006**, *12*, 5053–5059.

(38) Sprafke, J. K.; Stranks, S. D.; Warner, J. H.; Nicholas, R. J.; Anderson, H. L. *Angew. Chem., Int. Ed.* **2011**, *50*, 2313–2316.

6353

dx.doi.org/10.1021/ja500984k | *J. Am. Chem. Soc.* 2014, 136, 6348–6354

(39) Stranks, S. D.; Sprafke, J. K.; Anderson, H. L.; Nicholas, R. J. *ACS Nano* **2011**, *5*, 2307−2315.

(40) Hoffmann, M.; Wilson, C. J.; Odell, B.; Anderson, H. L. *Angew. Chem., Int. Ed.* **2007**, *46*, 3122−3125.

(41) Hoffmann, M.; Kärnbratt, J.; Chang, M.-H.; Herz, L. M.; Albinsson, B.; Anderson, H. L. *Angew. Chem., Int. Ed.* **2008**, *47*, 4993−4996.

(42) Winters, M. U.; Kärnbratt, J.; Eng, M.; Wilson, C. J.; Anderson, H. L.; Albinsson, B. *J. Phys. Chem. C* **2007**, *111*, 7192−7199.

(43) Ebbesen, T. W. *J. Phys. Chem. Solids* **1996**, *57*, 951−955.

(44) Palacin, T.; Le Khanh, H.; Jousselme, B.; Jégou, P.; Filoramo, A.; Ehli, C.; Guldi, D. M.; Campidelli, S. *J. Am. Chem. Soc.* **2009**, *131*, 15394−15402.

(45) Antoine, O.; Durand, R. *J. Appl. Electrochem.* **2000**, *30*, 839−844.